WARSAW UNIVERSITY OF TECHNOLOGY Index 351733
FACULTY OF CIVIL ENGINEERING
COMMITTEE FOR CIVIL AND WATER ENGINEERING
POLISH ACADEMY OF SCIENCES ISSN 1230-2945

DOI: 10.24425/ace.2023.147670

ARCHIVES OF CIVIL ENGINEERING

Vol. LXIX ISSUE 4 2023

pp. 459 –475

Research paper

Nonlinear static analysis of truss core sandwich beams in three-point bending test

Miroslaw Wesolowski[1], Mariusz Ruchwa[2], Sandris Rucevskis[3]

Abstract: An analysis of sandwich beams with truss core is an important issue in many fields of industry such as civil engineering, automotive, aerospace or maritime. The objective of the present study is a nonlinear static response of sandwich beams subjected to the three-point bending test configuration. The beams are composed of two parent components: upper and lower laminated face sheets (unidirectional tape) and a pyramidal truss core manufactured by means of 3D printing. A polyamide filament strengthened with chopped carbon fibres – CF-PA-12 is used for the core development. The both, experimental and numerical analyses are presented. A detailed numerical model of the sandwich beam was developed in Abaqus software. The numerical model considers modelling of the adhesive joint with an additional layer of material placed between the parent components of the beam. A continuum hybrid solid shell elements were used to model the adhesive layer. In addition, a special care was taken to use an appropriate material model for the CF-PA-12 filament. To do so, the uniaxial tensile tests were performed on 3D printed samples. Having acquired the test data, a hyperelastic material model was evaluated based on a curve fitting approach.

Keywords: additive manufacturing, numerical model, hyperelastic, sandwich beam, truss core

[1]DSc., PhD., Eng., Koszalin University of Technology, Faculty of Civil Engineering, Environment and Geodesy, ul. Śniadeckich 2, 75-453 Koszalin, Poland, e-mail: miroslaw.wesolowski@tu.koszalin.pl, ORCID: 0000-0001-8909-6608

[2]PhD., Eng., Koszalin University of Technology, Faculty of Civil Engineering, Environment and Geodesy, ul. Śniadeckich 2, 75-453 Koszalin, Poland, e-mail: mariusz.ruchwa@tu.koszalin.pl, ORCID: 0000-0003-2260-8423

[3]PhD., Eng., Riga Technical University, Faculty of Civil Engineering, 6B/6A Kipsalas Street, Riga, LV-1048, Latvia, e-mail: sandris.rucevskis@rtu.lv, ORCID: 0000-0002-0646-8064

1. Introduction

Many engineering problems related to the design or analysis of structures are often addressed through numerical analyses. This is especially the case when the structure is made of composite materials or hybrid metal composite materials. In such analyses a structure becomes highly anisotropic and its analytical treatment becomes very laborious. Among the large variability of composite structures, sandwich composites with a three dimensional (3D) truss core have recently gained the attention of the scientific community [1–6]. It is so due to the extraordinary engineering advantages of these type of composite structures. The above brings the need for a constant development and improvement of the numerical tools for analysing the composite structures behaviour.

The static behaviour of truss core sandwich structures is governed by the geometry of the parent components (outer lower and upper face sheets and internal core), as well as their constituent materials' properties. The face sheets mostly contribute to the bending stiffness of the sandwich structures, and are mainly used in the form of thin slabs, plates, or cylindrical shells. Two main groups of materials are used for the face sheet manufacturing, namely isotropic (aluminium or stainless steel) or anisotropic (laminated composites). The core of the above sandwich composites contributes to the shear stiffness and can be found to have different topology of 3D trusses, such as X-type [7], octet [8], tetrahedral cellular [9], and pyramidal [10]. For all of these types of truss geometries, the key parameter in terms of stiffness performance is a relative density, which is defined as the ratio of the truss volume enclosed in a unit cell to the total volume of that unit cell. The influence of the relative density on the static response of the truss core sandwich structures has been already extensively studied and its value of $\rho = 2 \div 7\%$ was defined as the most desirable [4, 7, 11]. A selection of a material used for core manufacturing is also an important factor in the overall core stiffness. The usual choice of the material is isotropic (aluminium, stainless steel, titanium alloys) or anisotropic (laminated composites strengthened with carbon fibres). However, a new group of materials can be found as a competitive replacement for the composite laminates. They are polymeric filaments used in the additive manufacturing process. Among them, the polyamide filaments strengthened with continuous or chopped carbon fibres are the most favourable. The variety of materials used for the core manufacturing implies the use of different constitutive material models for appropriate description of the core behaviour. For the isotropic materials a linear elastic or a linear elastic – ideal plastic material models are usually used [12]. For the case of laminated composites the applied models include elastic-plastic, failure, and post-failure behaviour [13]. For the polymeric filaments the choice of the material model is mostly case depended. As if for the ABS filament, for which the linear elastic – ideal plastic material model is wells suited [14], for the case of polyamide filaments with chopped carbon fibres the nonlinear elastic or nonlinear elastic – brittle material models seems to be a better choice. A possible approach for constitutive description of such polymeric materials is to use the hyperelastic material model which was originally dedicated for soft rubber-like material [15]. However, according to the Shore Hardness Scale [16], the polyamide material can be considered as an extra hard rubber material, for which the

hyperelastic theory also applies. In the hyperelastic theory the stress-strain relationship is derived from the strain energy potentials. In most cases, but not limited to, the energy potentials is described using the strain energy functions as Neo-Hookean [17], Mooney-Rivlin [18], Polynomial Form [19], Ogden [20], Marlow [21], Yeoh [22]. For a material under a combined load case the set of three static tests is required to correctly describe the hyperelastic material model. These test are uniaxial tension test, uniaxial compression test and simple shear/pure shear test. However, less number of tests can be used for a simple loading case [23].

A sandwich structure in its final form is manufactured by means of adhesive joints between the core and the face sheets. If all the parent materials are made of metal, the brazing or laser welding processes are used for the joints [24]. However, if the sandwich structure has the hybrid nature, e.g., laminated face sheets and 3D printed core, the joints must be provided by means of an adhesive material, e.g. epoxy resin. This may bring a relative displacements between the parent materials. For such a case, the adhesive joint shall be modelled in a way to account for the effects of joint compliance. The up to date studies on the truss core sandwich structures show that the modelling approach of the joints is mostly realized by an equivalent modelling [25, 26] or the Finite Element Method (FEM) [27, 28]. In FEM analyses, the bond between the parent materials is mostly defined as a tied contact (no relative displacement between parent materials is allowed at the joint locations) [29] or by the introduction of a mathematical model for adhesive joints (small displacements between parent materials are allowed at the joint locations) [30]. However the application of the above approaches is mostly limited for the cases where the parent components are made of the same type of material. The influence of the joints modelling on the dynamic response of an aluminium truss core/laminated face sheets sandwich beam has been studied in [31]. A significant results discrepancies have been reported between a tie contact joint modelling and a model with additional layers of adhesive material.

The purpose of the present study is to analyse a nonlinear static response of the pyramidal truss core sandwich structure in the form of a beam. The beam is composed of laminated face sheets and the pyramidal truss core manufactured by means of 3D printing (FDM). A novel approach to nonlinear material model application and the joints modelling is presented. Accordingly, the main effort is devoted to the modelling of the locally applied epoxy adhesive joints and a proper evaluation of a nonlinear material model (hyperelastic material model) for the 3D printed pyramidal core. The core was printed with a polyamide filament strengthened with a chopped carbon fibres CF-PA-12. The present analysis is limited to static nonlinear response with no fracture mechanics included, but the regions of the potential failure are indicated based on stress field. For this purpose a detailed three dimensional finite element model of the beam is developed with adhesive layers included. A numerical nonlinear static analysis was performed of the beam model in the three-point bending test configuration. The experimental measurements on real samples were also carried out and compered with the numerical results. In addition, a series of static uniaxial tension tests were performed on 3D printed samples in order to evaluate the hyperelastic material model properties.

2. Materials and methods

2.1. Samples manufacturing

The objects of the current study are sandwich composite beams. The sandwich beams were composed of two parent components as given in Fig. 1: (1) upper and lower face sheets made of a laminated carbon fibre reinforced plastic (CFRP); (2) a 3D printed pyramidal truss core made of a polyamide filament strengthened with chopped carbon fibres (CF-PA-12). The laminated face sheets were cut out of a long single-layer unidirectional CRFP tape. The tape was manufactured by means of a pultrusion process and was proven to be good candidates for flexural stiffness improvement [32]. The CF-PA-12 filament with a 15% by weight ratio of chopped fibres was used for the core development due to its good mechanical and thermal properties. The pyramidal truss core was assembled from separate pieces (longitudinal and transverse), which were manufactured by means of 3D printing in a heated and closed chamber. The advantage of the good thermal properties of the CF-PA-12 filament was taken and the printed pieces of the truss core were bonded together with a thermosetting epoxy adhesive (Loctite EA 9514) (Fig. 1a). After a curing process a continuous pyramidal truss core was obtained (Fig. 1b). The printing layout of the separate truss core pieces is given in Fig. 2 and the printing parameters were set as given

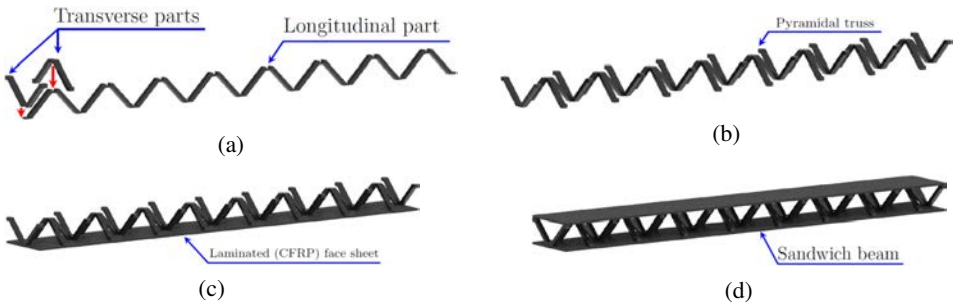

Fig. 1. Fabrication process of the truss core sandwich beam: a), b) polyamide pyramidal truss core assembly; c), d) the sandwich beam assembly with laminated face sheets and pyramidal core

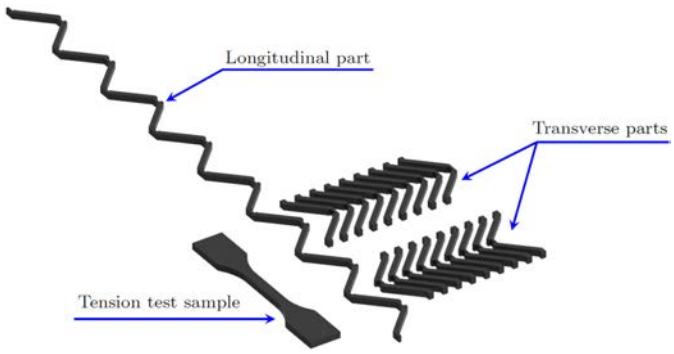

Fig. 2. The 3D printing pattern of the truss core parts and the samples for static tests

in Table 1. In a final step, the parent components were bonded together to form a sandwich beam (Fig. 1c, 1d). In the bonding process, the same thermosetting epoxy adhesive was used as for the core assembly.

Table 1. 3D printing process parameters for the truss core parts and tensile test samples

Parameter	Value
Layer thickness	0.2 [mm]
Nozzle diameter	0.4 [mm]
Infill	100.0 [%]
Infill pattern (raster)	Rectilinear [+45 / –45] deg
Nozzle temperature	270.0°C
Bed (table) temperature	105.0°C
Chamber temperature	50.0°C

The epoxy adhesive was applied locally at the contact spots between the sheets and the core. Two samples were manufactured for experimental investigation with characteristic dimensions as given in Table 2. The geometry of the beam and the single unit cell are given in Fig. 3. For the given unit cell geometry, the relative density of the core was obtained as $\rho = 3.05\%$ [33]. Besides the sandwich beams, samples for the static tensile tests were manufactured. The samples were 3D printed with the same filament, pattern (Fig. 2), and printing parameters (Table 1) as the truss core parts. The type IV geometry of the sample was taken (Fig. 4) according to the ASTM standard [34]. Ten samples were fabricated for the tensile tests.

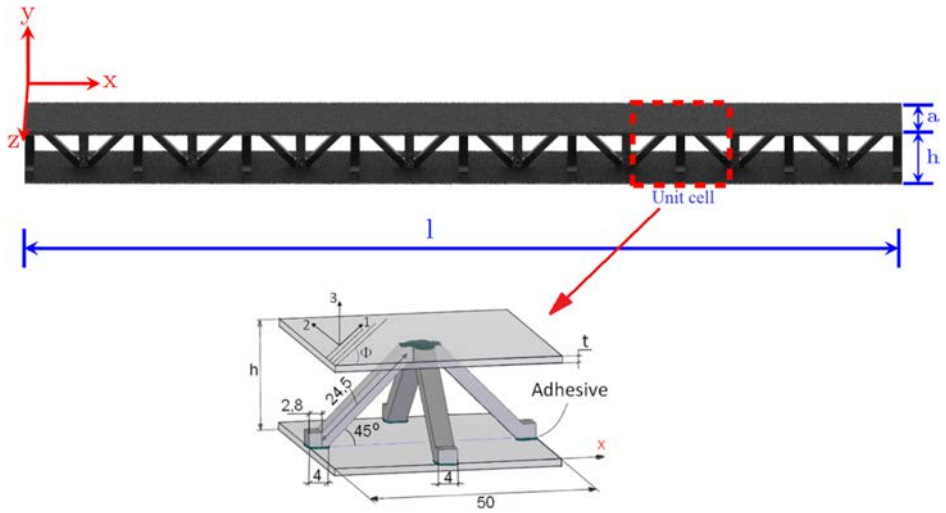

Fig. 3. Characteristic dimensions of the sandwich beam and a unit cell

Table 2. Characteristic dimensions of the fabricated sandwich beams

Sample	l [mm]	a [mm]	h [mm]	t [mm]	Φ [deg]
Sandwich 1	386.4	50.0	22.76	1.4	0.0
Sandwich 2	386.1	50.0	22.78	1.4	0.0

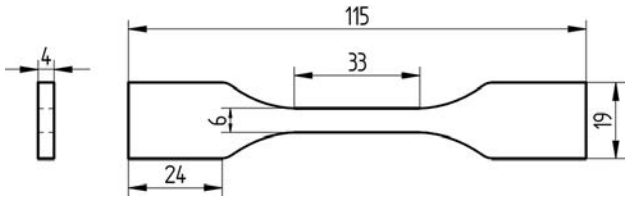

Fig. 4. Dimensions of the tensile test sample type IV [34] fabricated by means of 3D printing

2.2. Numerical model

The Finite Element Method (FEM) was used to developed the model of the sandwich beam. The Abaqus software was used as a pre- and post-processor. For a modelling purpose a global Cartesian coordinate system (x, y, z) was defined for the beam as given in Fig. 3. For the CRFP laminated face sheets a lamina coordinate system (1, 2, 3) was defined with the direction 1 along the fibres of the tape, 2 transverse to this direction, and 3 through the thickness direction.

A lamination angle (Φ) of the fibres was defined between the x-axis and the 1-axis (Fig. 3). The FEM model was assumed to be an assembly of three components (instances), namely laminated face sheets, the 3D printed pyramidal truss core and the adhesive material. The laminated tape used for the face sheets was considered as a thin and narrow plate.

For such a case it is customary to build the numerical model using single layer shell elements. To fulfil the above assumptions, the S4R shell elements with an orthotropic elastic material model were used. The 3D printed pyramidal core was considered as a solid 3D body (Fig. 5a). No adhesive connections between the longitudinal and transverse parts of the core were modelled. In order to discretize the 3D body, 8-node linear brick elements C3D8RH were used with an isotropic hyperelastic material model (Fig. 5b). A single adhesive joint between the pyramidal truss and the face sheets had the form of a thin layer of an additional material. Consequently, the continuum hybrid solid-shell elements SC8R were selected for the discretization of the adhesive layer. The SC8R elements behave like three-dimensional continuum solids, but they have kinematic and constitutive behaviour that is similar to conventional shell elements. The advantage of the SC8R elements is that they exhibit fast element convergence along the thickness direction. For the adhesive layer, one element in the thickness direction was sufficient in order to gain the results convergence (Fig. 5c). The isotropic elastic material model was applied for all of the adhesive joints.

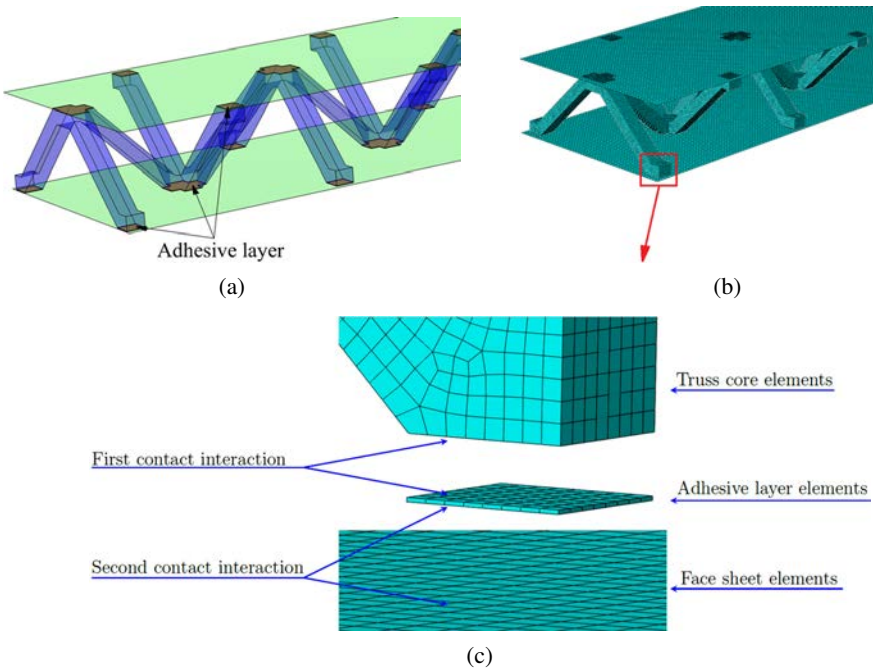

Fig. 5. Development procedure of the numerical model: a) Parent materials assembly; b) Associated mesh; c) Joint modelling with the adhesive layer

The material properties of the model components were established in the following way. In case of the laminated face sheets, the elastic material's properties were estimated by means of an inverse technique as described in [35–37]. The elastic properties were then associated with the corresponding axes (1, 2, 3) of the lamina's coordinate system of the face sheets model. The elastic properties of the adhesive material was adopted based on the manufacturer's technical data sheet. The material properties of the both parent components are listed in Table 3. The material properties of the 3D printed truss core were assumed to be nonlinear-elastic. For such a case the hyperelastic material model was applied in the analysis. The evaluation process of the hyperelastic material model is described in the subsequent paragraph.

Table 3. Elastic properties of the parent components

Parent Component	Material	E [GPa]	E_1 [GPa]	E_2 [GPa]	G_{12} [GPa]	G_{13} [GPa]	G_{23} [GPa]	ν_{12}	ν	Ultimate Shear [MPa]
Face sheet	CFRP	–	142.2	10.5	7.8	7.8	3.8	0.3	–	–
Adhesive	Epoxy	1.46	–	–	–	–	–	–	0.25	2.0÷30.0

2.2.1. Hyperelastic material model

Based on the hyperelastic theory [15], the stress-strain relationship of hard polymeric materials can be derived from the strain energy potentials as:

$$W = (\lambda_1, \lambda_2, \lambda_3) \tag{2.1}$$

where: λ_i – the principal stretches with $i = 1, 2, 3$.

At first, the Ogden strain energy function is used to describe the behaviour of the 3D printed core. The Odgen function is based on reduced principal stretches derived from a deviatoric part of the left Cauchy–Green tensor. It is implemented in the Abaqus [38] as:

$$W = \sum_{i=1}^{N} \frac{2\mu_i}{\alpha_i^2} \left(\overline{\lambda}_1^{\alpha_i} + \overline{\lambda}_2^{\alpha_i} + \overline{\lambda}_3^{\alpha_i} - 3 \right) + \sum_{i=1}^{N} \frac{1}{D_i} (J^{el} - 1)^{2i} \tag{2.2}$$

where: J^{el} – the elastic volume ratio, $\overline{\lambda}_i$ – the reduced principal stretches, N – the order of the Ogden function, μ_i – the material constants related to shear modulus and expressed in [MPa], α_i – a dimensionless quantities, D_i – the incompressibility parameters used to indicate the volume change and expressed in [MPa].

The reduced principal stretches are related to the principal stretches as $\overline{\lambda}_i = J^{-\frac{1}{3}} \lambda_i$, with $J = (\lambda_1 \lambda_2 \lambda_3)^{\frac{1}{2}}$. Both, the μ_i and α_i must be identified, where the initial value of the shear modulus is set as $\mu_0 = \sum_{i=1}^{N} \mu_i$. The material constants can be identified using as many test data as many deformation modes will appear in a structure during the FEM analysis. Therefore, the crucial point is to acquire data which are most adequate to that deformation modes. The elements of the 3D printed core deform axially while the sandwich beam is subjected to the bending. On that reason to identify the material constants, the data of stress-strain curve from uniaxial tension test was only used. Having selected the order of the strain energy potential function in the form of Eq. (2.2), the material coefficients are found by solving an optimization problem with a built in Abaqus tool. The optimization is achieved by minimizing the cost function expressed as a cumulative relative error between experimental data (σ_{EXP}) and model predicted data (σ_{FEM}). The cost function is given as:

$$\Delta = \sum_{k=1}^{n} \left(\frac{(\sigma_{\text{EXP}}^k - \sigma_{\text{FEM}}^k)}{\sigma_{\text{EXP}}^k} \right)^2 \tag{2.3}$$

where: n – the number of measurement points on a stress–strain curve.

For the Ogden function a nonlinear regression method is used to minimize the cost function with the optimal values of the material constants. For the current study, the lack of the volumetric tests was recompensed by introducing the Poisson's ratio of $\nu = 0.4$ for the CF-PA-12 material.

Another approach to the strain energy function treatment was proposed by the Marlow's model [39]. The Marlow's model uses scalar functions in defining the material behaviour instead of material's coefficients. The model assumes that the strain energy density depends

only on the first deviatoric strain invariant ($\bar{I}_1 = \bar{\lambda}_1^2 + \bar{\lambda}_2^2 + \bar{\lambda}_3^2$) and can be decomposed into a deviatoric W_{dev} and a volumetric W_{vol} part (required for a compressible case only) as [21, 39]:

$$W = W_{\text{dev}}\left(\bar{I}_1\right) + W_{\text{vol}}(J) \tag{2.4}$$

The implementation of the Marlow's model in Abaqus software is straightforward. It requires the stress–strain curves provided in the tabular form which come from one of the following tension tests: uniaxial, equibiaxial, or planar. For a compressible models, a volumetric test would be also required. The usefulness of this approach is that the material model built on the provided data is reproduced exactly during the solution process.

2.2.2. Model assembly and solution type

The model of the sandwich beam was assembled from the separate instances based on the contact definition. The length $l = 386.25$ mm of the beam was set as the mean value of the beams' lengths given in Table 2. The rest of the beam's dimensions were set as: $a = 50.0$ mm, $h = 22.8$ mm and $t = 1.4$ mm. The lamination angle was set to $\Phi = 0$ deg. The thickness of the adhesive layers was set to 0.1 mm. The assembly of the sandwich beam with the adhesive layers was performed by means of the two tie contact interactions at each adhesive joint. The first contact was defined between the inner surface of the adhesive layer and the outer surface of the 3D printed pyramidal truss core. The second contact was defined between the outer surface of the adhesive layer and the inner surface of the laminated face sheets. The model development procedure is given schematically in Fig. 5c.

In order to simulate the three-point bending configuration, two supports were modelled and a cross head. The translation degrees of freedom of the supports were blocked on the direction x, y, z. For the cross head, the translation on y direction was allowed. The surface to surface contacts were modelled between the beam and the supports as well as the cross head (Fig. 6). In order to gain a solution stability a friction parameter of 0.01 was introduced. The beam deflection and supports reactions were achieved by imposing an initial displacement of 2.2 mm of the cross head in the vertical direction (along y axis). The convergence study was performed versus elements size and the stability of the solution was achieved for: 38600 S4R total elements for the both face sheets, 154832 C3D8RH

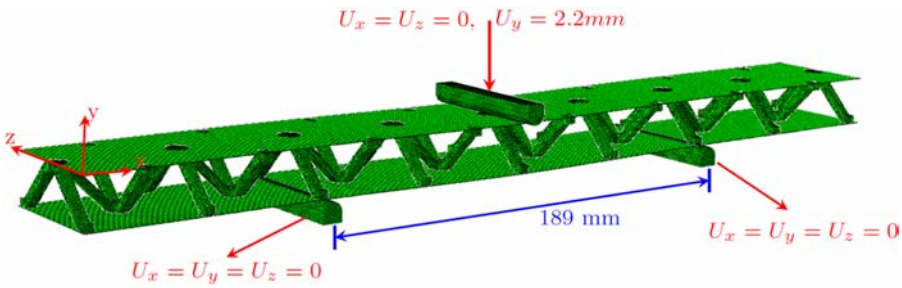

Fig. 6. Three-point bending test FEM model of the sandwich beam

elements for the 3D printed pyramidal core, 5376 SC8R elements for the adhesive joints. In total 198808 finite elements was used to build the numerical model of the sandwich beam. For the current problem, the nonlinear static solution was selected and the analysis was performed. The history of the total reaction forces at the supports versus the beam's mid span displacement was stored.

2.3. Experimental tests

2.3.1. Uniaxial tensile test

A test setup was developed according to [34] for the uniaxial tensile tests of the samples fabricated by means of 3D printing (Fig. 7). The tensile testing machine Zwick/Roell was used with a load cell of 10 kN. The specimens were tested at room temperature (22°C) with the cross head speed of 1.5 mm/min. The nominal strain data were obtained from the clip extensometer Zwick/Roell with an initial gauge length of $s_0 = 25$ mm. The strain at each loading stage i was calculated as: $\varepsilon_i = s_i/s_0$, where s_i is the extensometer length change given in mm. Based on the load cell force and the nominal strain, the 10 stress-strain curves were derived.

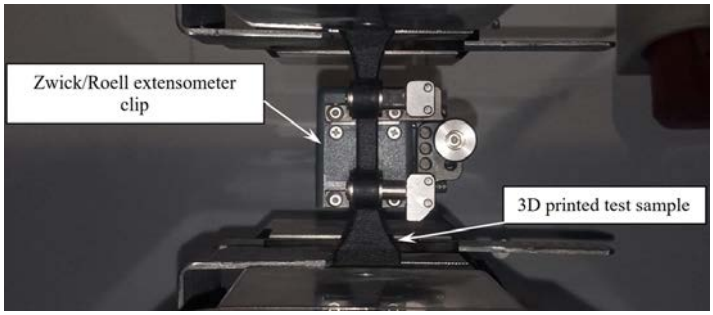

Fig. 7. Uniaxial tensile test set-up with Zwick/Roell machine

2.3.2. Three-point bending test

The realisation of the laboratory testing in a three-point bending configuration was done on a static machine combined with an optical noncontact sensing of deformations (Fig. 8). The loading was provided by the INSPECT 600 machine having the force range of $0 \div 600$ kN throughout the cross head. The loading was applied to the beam in the half span length between the supports. The span between the supports was set to 189 mm. The tests were conducted in accordance to [40] in room temperature. The cross head displacement speed was set up to 6 mm/min. Force versus displacement was recorded continuously by optical sensing device ARAMIS in the middle of the beam as well as in several points labelled with optical markers. The initial failure was recorded with the ARAMIS system together with the corresponding force and displacement data.

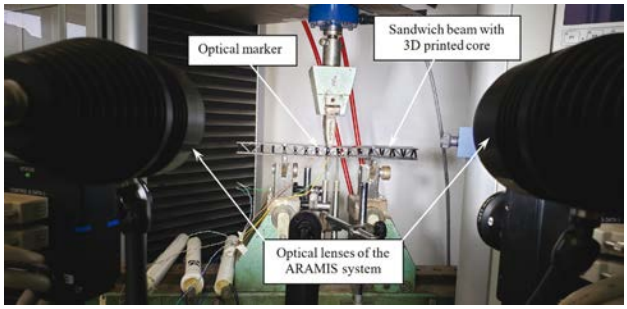

Fig. 8. Three-point bending test set-up with INSPECT-600 and ARAMIS system

3. Results

The experimental tests were performed on the developed samples. The both, printed tensile samples and the sandwich beams were tested successfully. The stress-strain curves of the tensile samples were developed based on the 10 tensile static tests and are plotted in Fig. 9a. The average stress-strain curve was then developed out of the 10 samples (Fig. 9b). The obtained stress-strain curve clearly indicates the nonlinear behaviour of the CF-PA-12 material. The results of the three-point bending tests of the sandwich beams were stored for the 2 developed samples (Fig. 10a). For each sample, the testing procedure was terminating after the first failure mode has occurred. By the samples inspection, it was noticed that the first failure mode was the break (collapse) of the 3D printed truss longitudinal part (Fig. 11a). The fact of the truss core failure implies that the adhesive joints are able to withstand the applied load prior any other failure mode. Next, the averaged test data from the tensile tests were imported into the Abaqus software and the evaluation of the hyperelastic material coefficients was run. Two types of strain energies were evaluated, namely Ogden and Marlow. For the Ogden function the process was run for $N = 2$ and $N = 3$. The optimization processes resulted with the stress-strain curve given in Fig. 10b and material

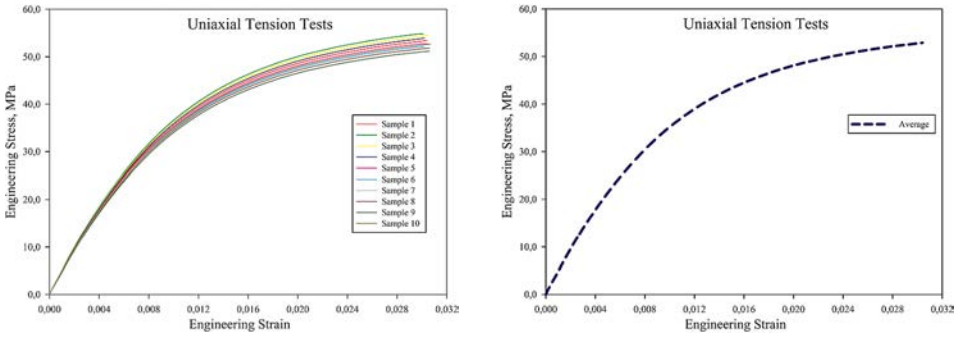

(a) (b)

Fig. 9. Uniaxial tension tests results: a) all tested samples; b) average curve

coefficients (for Ogden functions only) listed in Table 4. The obtained material coefficients were used in the material card of the 3D printed truss core numerical model. In case of the Marlow function the Abaqus solver followed the imported stress-strain cure during solution process so that no additional coefficients were required. The static nonlinear FEM analysis of the sandwich beam model was run. The load – displacement curve was plotted for the mid span point of the numerical model (Fig. 10a).

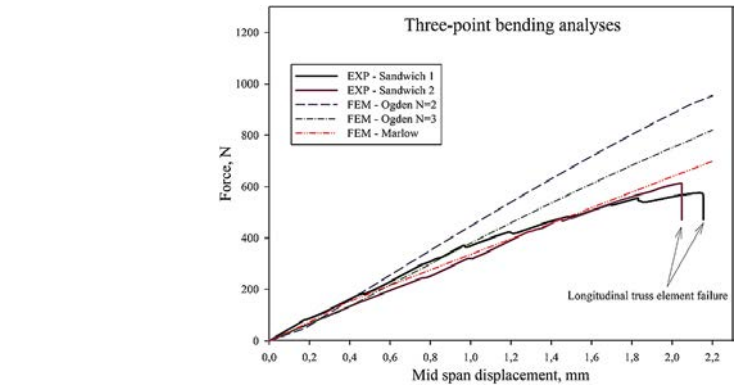

(a)

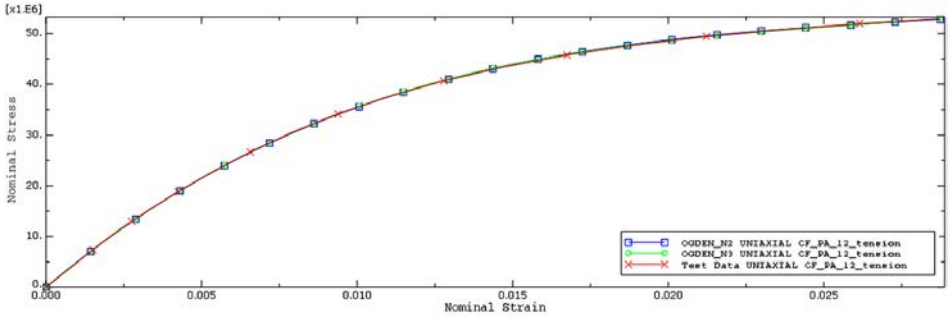

(b)

Fig. 10. Comparison of the three-point bending test analyses: a) Experimental versus calculated results; b) Abaqus fit of the Odgen function

Table 4. Ogden strain energy function coefficients

Function order	μ_1 [MPa]	α_1[–]	D_1 [MPa]	μ_2 [MPa]	α_2[–]	D_2 [MPa]	μ_3 [MPa]	α_3 [–]	D_3 [MPa]	Δ %
$N = 2$	$-354.0 \cdot 10^2$	–13.40	$2.47 \cdot 10^{-16}$	$371.0 \cdot 10^2$	–19.54	0.0	–	–	–	0.87
$N = 3$	$-815.0 \cdot 10^3$	2.00	$2.48 \cdot 10^{-16}$	$504.0 \cdot 10^3$	4.00	0.0	$313.0 \cdot 10^3$	–2.00	0.0	0.82

By the comparison of the experimental curves and the corresponding numerical results it can be observed that the best agreement was found for the numerical solution with the Marlow strain energy function. However, a consistent results can be also found for the Ogden $N = 3$ function but only for the lower displacement level (approximately a halfway prior to the failure). The stress field developed on the 3D printed truss core for the assumed beam deflection is given in Fig. 11a and Fig. 11c. The stress map correctly indicates the zone and stress value of a possible truss failure as it was the case during experimental tests (Fig. 11b). In addition, the modelling of the adhesive layers resulted in the deep insight of the stress and strain field developed in the layers. As given in Fig. 11d the shear stress developed in the adhesive layers prior the truss failure is considerably less than the ultimate shear stress provided in Table 3. The above agree with the experimental results where none of the adhesive joints have failed.

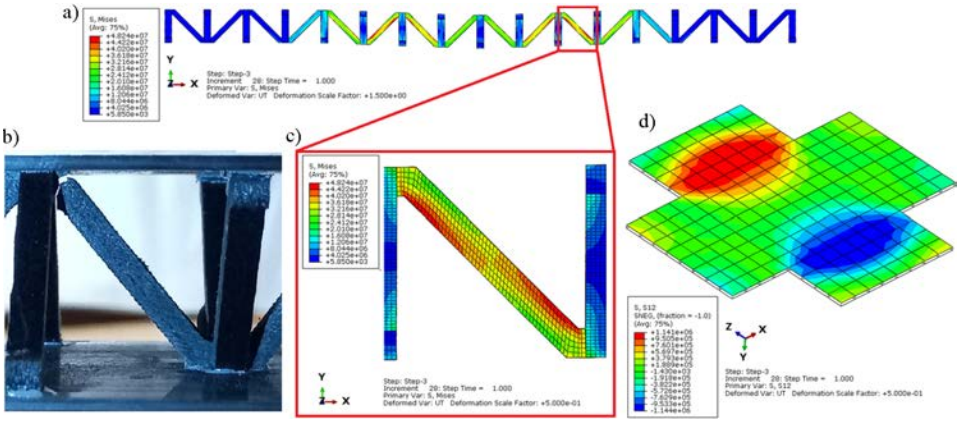

Fig. 11. Three-point bending test results: a) Calculated stress filed on the 3D printed truss core; b) First failure mode from the experimental tests; c) FEM stress field indicates possible location of the failure; d) Shear stress at the selected adhesive joint. All stresses in [Pa]

4. Conclusions

The experimental and numerical analyses of the sandwich beams with the 3D printed truss core have been performed successfully. On the basis of the obtained results, the current research can be summarized be following conclusions:

1. The material model used for the truss core modelling has a crucial importance for the results convergence with the experimental test.
2. A hyperelastic material model proposed for the polyamide filament strengthen with chopped carbon fibres seems to be adequate for a given problem.
3. For a low strain level of the truss core, the Ogden strain energy function of the order $N = 3$ or Marlow material model for higher strain level can be used based on a single uniaxial tensile test. However, despite the usefulness of the Marlow model, it can be only applied with a single tensile test data.

4. An additional research activities shall be made focusing on a static response of the sandwich beam under a combined loading case, for which more tensile test would be required in developing the hyperplastic material model.
5. The reliability of the numerical model was considerably enhanced by the modelling of the additional layer of adhesive material.

References

[1] M. Ruzzene, "Vibration and sound radiation of sandwich beams with honeycomb truss core", *Journal of Sound and Vibration*, vol. 277, no. 4–5, pp. 741–763, 2004, doi: 10.1016/j.jsv.2003.09.026.

[2] L.J Feng, J. Xiong, L.H. Yang, G.C. Yu, W. Yang, and L.Z. Wu, "Shear and bending performance of new type enhanced lattice truss structures", *International Journal of Mechanical Sciences*, vol. 134, pp. 589–598, 2017, doi: 10.1016/j.ijmecsci.2017.10.045.

[3] J. Wang, W. Liu, S. Kang, T. Ma, Z. Wang, W. Yuan, H. Song, and C. Huang, "Compression performances and failure maps of sandwich cylinders with pyramidal truss cores obtained through geometric mapping and snap-fit method", *Composite Structures*, vol. 226, pp. 1–10, 2019, doi: 10.1016/j.compstruct.2019.111212.

[4] J. Xiong, L. Ma, S. Pan, L. Wu, J. Papadopoulos, and A. Vaziri, "Shear and bending performance of carbon fiber composite sandwich panels with pyramidal truss cores", *Acta Materialia*, vol. 60, no. 4, pp. 1455–1466, 2012, doi: 10.1016/j.actamat.2011.11.028.

[5] G.D. Xu, F. Yang, T. Zeng, S. Cheng, and Z.H. Wang, "Bending behavior of graded corrugated truss core composite sandwich beams", *Composite Structures*, vol. 138, pp. 342–351, 2016, doi: 10.1016/j.compstruct.2015.11.057.

[6] G.D. Xu, T. Zeng, S. Cheng, X.H. Wang, and K. Zhang, "Free vibration of composite sandwich beam with graded corrugated lattice core", *Composite Structures*, vol. 229, pp. 1–7, 2019, doi: 10.1016/j.compstruct.2019.111466.

[7] W. Yang, J. Xiong, L.J. Feng, C. Pei, and L.Z. Wu, "Fabrication and mechanical properties of three-dimensional enhanced lattice truss sandwich structures", *Journal of Sandwich Structures & Materials*, vol, 22, no. 5, pp. 1–18, 2018, doi: 10.1177/1099636218789602.

[8] L. Dong, V. Deshpande, and H. Wadley, "Mechanical response of Ti-6Al-4V octet-truss lattice structures", *International Journal of Solids and Structures*, vol. 60–61, pp. 107–124, 2015, doi: 10.1016/j.ijsolstr.2015.02.020.

[9] J. Mei, J.Y. Liu, and J.L Liu, "A novel fabrication method and mechanical behavior of all composite tetrahedral truss core sandwich panel", *Composites Part A: Applied Science and Manufacturing*, vol. 102, pp. 28–39, 2017, doi: 10.1016/j.compositesa.2017.07.020.

[10] K. Wei, R.J. He, X.M. Cheng, Y. Pei, R. Zhang, and D. Fang, "Fabrication and heat transfer characteristics of C/SiC pyramidal core lattice sandwich panel", *Applied Thermal Engineering*, vol. 81, pp. 10–17, 2015, doi: 10.1016/j.applthermaleng.2015.02.012.

[11] G. Qi, B. Ji, and L. Ma, "Mechanical response of pyramidal lattice truss core sandwich structures by additive manufacturing", *Mechanics of Advanced Materials and Structures*, vol. 26, no. 15, pp. 1298–1306, 2019, doi: 10.1080/15376494.2018.1432805.

[12] P. Baranowski, P. Płatek, A. Antolak-Dudka, M. Sarzyński, M. Kucewicz, T. Durejko, J. Małachowski, J. Janiszewski, and T. Czujko, "Deformation of honeycomb cellular structures manufactured with Laser Engineered Net Shaping (LENS) technology under quasi-static loading: Experimental testing and simulation", *Additive Manufacturing*, vol. 25, pp. 307–316, 2019, doi: 10.1016/j.addma.2018.11.018.

[13] R.M. Jones, *Mechanics of composite materials,* 2nd ed. Taylor and Francis CRC Press, 1999.

[14] M. Kucewicz, P. Baranowski, J. Małachowski, A. Popławski, and P. Płatek, "Modelling, and characterization of 3D printed cellular structures", *Materials and Design*, vol. 142, pp. 177–189, 2018, doi: 10.1016/j.matdes.2018.01.028.

[15] R.W. Ogden, "Large deformation isotropic elasticity – on the correlation of theory and experiment for compressible rubberlike solids", *Proceedings of the Royal Society A*, vol. 326, pp. 567–583, 1972, doi: 10.1098/ rspa.1972.0026.

[16] ASTM D2240-15(2021) Standard Test Method for Rubber Property – Durometer Hardness. American Society for Testing and Materials Standards, 2021.

[17] H. Bechir, L. Chevalier, M. Chaouche, and K. Boufala, "Hyperelastic constitutive model for rubber-like materials based on the first Seth strain measures invariant", *European Journal of Mechanics – A/Solids*, vol. 25, no. 1, pp. 110–124, 2006, doi: 10.1016/j.euromechsol.2005.03.005.

[18] I.S. Liu, "A note on the Mooney–Rivlin material model", *Continuum Mechanics and Thermodynamics*, vol. 24, pp. 583–590, 2012, doi: 10.1007/s00161-011-0197-6.

[19] R. Cai, F. Holweck, Z.Q. Feng, and F. Peyraut, "A new hyperelastic model for anisotropic hyperelastic materials with one fiber family", *International Journal of Solids and Structures*, vol. 84, pp. 1–16, 2016, doi: 10.1016/j.ijsolstr.2015.11.008.

[20] Y. Yao, S. Chen, and Z. Huang, "A generalized Ogden model for the compressibility of rubber-like solids", *Philosophical Transactions of the Royal Society A*, vol. 380, pp. 1–18, 2022, doi: 10.1098/rsta.2021.0320.

[21] O. Hesebeck, "Transformation of Test Data for the Specification of a Viscoelastic Marlow Model", *Solids*, vol. 1, no. 1, pp. 2–15, 2020, doi: 10.3390/solids1010002.

[22] O.H. Yeoh, "Some forms of the strain energy function for Rubber", *Rubber Chemistry and Technology*, vol. 66, no. 5, pp. 754–771, 1993, doi: 10.5254/1.3538343.

[23] Y. Gorash, T. Comlekci, and R. Hamilton, "CAE-Based application for identification and verification of hyperelastic parameters", *Proceedings of the Institution of Mechanical Engineers, Part L: Journal of Materials: Design and Applications*, vol. 231, no. 7, pp. 611–626, 2015, doi: 10.1177/1464420715604004.

[24] V.S. Deshpande and N.A. Fleck, "Collapse of truss core sandwich beams in 3-point bending", *International Journal of Solids and Structures*, vol. 38, no. 36-37, pp. 6275–6305, 2001, doi: 10.1016/S0020-7683(01)00103-2.

[25] M.R. O'Masta, L. Dong, L. St-Pierre, H.N.G. Wadley, and V.S. Deshpande, "The fracture toughness of octet-truss lattices", *Journal of the Mechanics and Physics of Solids*, vol. 98, pp. 271–289, 2017, doi: 10.1016/ j.jmps.2016.09.009.

[26] T. George, V.S. Deshpande, and H.N.G. Wadley, "Hybrid carbon fiber composite lattice truss structures", *Composites Part A: Applied Science and Manufacturing*, vol. 65, pp. 135–147, 2014, doi: 10.1016/j.compositesa. 2014.06.011.

[27] X. Zhang, X. Jin, G. Xie, and H. Yan, "Thermo-Fluidic Comparison between Sandwich Panels with Tetrahedral Lattice Cores Fabricated by Casting and Metal Sheet Folding", *Energies*, vol. 10, no. 7, pp. 1–17, 2017, doi: 10.3390/en10070906.

[28] S. Yin, H. Chen, Y. Wu, Y. Li, and J. Xu, "Introducing composite lattice core sandwich structure as an alternative proposal for engine hood", *Composite Structures*, vol. 201, pp. 131–140, 2018, doi: 10.1016/ j.compstruct.2018.06.038.

[29] J.S. Yang, L. Ma, M. Chaves-Vargas, T.X. Huang, K.U. Schröder, R. Schmidt, and L.Z. Wu, "Influence of manufacturing defects on modal properties of composite pyramidal truss-like core sandwich cylindrical panels", *Composites Science and Technology*, vol. 147, pp. 89–99, 2017, doi: 10.1016/j.compscitech.2017.05.007.

[30] M. Xu and Z. Qiu, "Free vibration analysis and optimization of composite lattice truss core sandwich beams with interval parameters", *Composite Structures*, vol. 106, pp. 85–95, 2013, doi: 10.1016/j.compstruct.2013.05.048.

[31] M. Wesolowski M, M. Ruchwa, E. Skukis, and A. Kovalovs, "Numerical and Experimental Extraction of Dynamic Parameters for Pyramidal Truss Core Sandwich Beams with Laminated Face Sheets", *Materials*, vol. 13, no. 22, pp. 1–17, 2020, doi: 10.3390/ma13225199.

[32] W. Głodkowska and M. Ruchwa, "Static Analysis of Reinforced Concrete Beams Strengthened with CFRP Composites", *Archives of Civil Engineering*, vol. 56, no. 2, pp. 111–122, 2010, doi: 10.2478/v.10169-010-0006-9.

[33] G. Zhang, B. Wang, L. Ma, J. Xiong, and L. Wu, "Response of sandwich structures with pyramidal truss cores under the compression and impact loading", *Composite Structures*, vol. 100, pp. 451–463, 2013, doi: 10.1016/j.compstruct.2013.01.012.

[34] ASTM D D638–14 Standard Test Method for Tensile Properties of Plastics. American Society for Testing and Materials Standards, 2014.

[35] E. Barkanov, M. Wesolowski, W. Hufenbach, and M. Dannemann, "An effectiveness improvement of the inverse technique based on vibration tests", *Computers & Structures*, vol. 146, pp. 152–162, 2015, doi: 10.1016/j.compstruc.2014.10.006.

[36] M. Wesolowski and E. Barkanov, "Improving material damping characterization of a laminated plate", *Journal of Sound and Vibration*, vol. 462, pp. 1–12, 2019, doi: 10.1016/j.jsv.2019.114928.

[37] P. Kłosowski and A. Zagubień, "Analysis of material properties of technical fabric for hanging roofs and pneumatic shells", *Archives of Civil Engineering*, vol. 49, no. 3, pp. 277–294, 2003.

[38] Simulia/Abaqus, *Abaqus Reference Manuals*. 2016.

[39] R.S. Marlow, "A general first-invariant hyperelastic constitutive model", in *Constitutive Models for Rubber II*. Lisse, The Netherlands: Balkema, 2003, pp. 157–160.

[40] ASTM C393/C393M–20 Standard Test Method for Core Shear Properties of Sandwich Constructions by Beam Flexure. American Society for Testing and Materials Standards, 2020.

Nieliniowa analiza statyczna konstrukcji przekładkowej z wypełnieniem kratownicowym (typu sandwich) wg. trzypunktowego schematu zginania

Słowa kluczowe: technika przyrostowa, model numeryczny, hipersprężystość, belka przekładkowa, wypełnienie kratownicowe

Streszczenie:

Kompozytowe struktury przekładkowe z wypełnieniem kratownicowym (typu sandwich) są wytwarzane w postaci płyt, belek, oraz powłok cylindrycznych. Kompozyty te zbudowane są głównie z dwóch materiałów macierzystych, tj. okładzin zewnętrznych w postaci cienkich płyt lub taśm oraz wypełnienia wewnętrznego o geometrii przestrzennej kratownicy. Struktury te mogą być traktowane jako elementy konstrukcyjne ze względu na ich znakomite wskaźniki sztywności i wytrzymałości w stosunku do masy. Ponadto, ich komórkowa budowa poprawia możliwości wentylacyjne oraz umożliwia prowadzenia instalacji pomiędzy poszczególnymi komórkami całej struktury. Powoduje to, że oprócz funkcji nośnych, struktury te stanowią również elementy funkcjonalne. Zalety struktur przekładowych przyczyniły się do zintensyfikowania badań naukowych w zakresie analiz statycznych. Jako, że struktury te stanowią kompozyt, ich właściwości mechaniczne przyjmują różnorodne cechy w zależności od schematu obciążenia. Pociąga to za sobą dodatkowe trudności w procesie modelowania takich konstrukcji ze względu na bardzo szeroki zakres materiałów stosowanych do ich budowy oraz połączeń między nimi. Różnorodność ta przejawia się już w doborze okładzin zewnętrznych, które są wykonywane z trzech grup materiałów, tj. metali lub ich stopów (np. aluminium), laminatów warstwowych (np. laminaty włókniste), materiałów organicznych (np. sklejka). Kolejną kwestią jest materiał stosowany na budowę komórkowej warstwy wypełnienia. Ograniczając się do jednej geometrii tej warstwy, tj. do postaci przestrzennej kratownicy, materiałami stosowanymi do ich budowy, poza wyżej wspomnianymi, są polimery wytwarzane techniką przyrostową. Niestety zdecydowana większość opracowań naukowych pozostawia bez komentarza kwestie modelowania oraz nośności połączeń adhezyjnych w powyższych strukturach.

W bieżącej pracy założono przeprowadzenie analizy statycznej wg schematu trzypunktowego zginania. W procesie budowy modelu numerycznego uwzględniono połączenia klejone pomiędzy elementami macierzystymi belki poprzez wprowadzenie dodatkowego materiału adhezyjnego. Do modelowania polimerowego wypełnienia kratownicowego (CF-PA-12) zastosowano hipersprężysty model materiału. Parametry sprężyste modelu materiałowego oszacowano na podstawie statycznej

próby rozciągania próbek wytworzonych techniką przyrostową. Weryfikacja poprawności opracowanego modelu MES przeprowadzona została na podstawie porównania obliczeń numerycznych z przeprowadzonymi pomiarami laboratoryjnymi, uzyskując dużą zbieżność wyników. Przeprowadzone badania pozwoliły na opracowanie modelu numerycznego belki przekładkowej z uwzględnieniem warstwy adhezyjnej. Wykony model numeryczny belki może służyć do prognozowania jej odpowiedzi statycznej. Zastosowanie kontynualnych elementów skończonych pozwoliło na znaczną redukcję ilości elementów po grubości warstwy adhezyjnej.

Received: 2023-07-19, Revised: 2023-08-25